



ACADEMIC
PRESS

Available online at www.sciencedirect.com

SCIENCE @ DIRECT®

Journal of Magnetic Resonance 162 (2003) 364–370

JMR
Journal of
Magnetic Resonance

www.elsevier.com/locate/jmr

Separation of velocity distribution and diffusion using PFG NMR

A. Gottwald, P. Kuran, and U. Scheler*

Institute for Polymer Research Dresden, Hohe Strasse 6, Dresden D-01069, Germany

Received 21 October 2002; revised 17 March 2003

Abstract

Pulsed field gradient (PFG) NMR is applied to investigate flow processes. In this case the NMR signal experiences phase modulation due to flow and signal attenuation due to the distribution of velocities. The velocity distribution consists of one part originating from diffusion and of a second part, the distribution of the directed motion. The usual PFG-experiment in which the gradient strength is incremented cannot distinguish between both. Incrementing velocity at constant gradient strength keeps the contribution from diffusion constant but changes the absolute width of the velocity distribution. So the signal is attenuated again, but only due to the distribution of the directed motion. The phase modulation as a signature of flow is not affected by this strategy, because velocity and gradient strength are Fourier conjugated. The key advantage of this approach is the possibility of measuring very low velocities, which only cause a very slight phase modulation that is easily covered by diffusion. The method is discussed here for very slow flow in a rheometer cell.

© 2003 Elsevier Science (USA). All rights reserved.

Keywords: Velocity distribution; Diffusion; Rheological NMR; PFG NMR; Coherent and incoherent motion

1. Introduction

Realizing the number of technical applications where flowing media are involved (e.g., transporting liquids through tubes, mixing of (im)miscible compounds in stirring reactors, or mixing and transporting polymer melts in extruders, mixers, or other processing apparatus) several methods are commonly used to investigate flow processes, such as laser anemometry and high-speed videography. The pulsed field gradient NMR (PFG NMR) is another one of these methods [1,2]. PFG NMR is also used for diffusion measurements [3,4]. Usually, it is applied to probe either diffusion or flow.

The motion in a realistic flowing liquid consists of coherent and incoherent contributions. The coherent one is the directed flow, which results in a phase modulation of the NMR signal. All incoherent contributions result in a signal attenuation. Thus, in the classic PFG experiment coherent and incoherent motion can be separated by post-processing [1], provided that the attenuation is not much stronger than the phase modulation.

The separation of the different incoherent contributions is not possible by a single experiment so far. These contributions can be subdivided further into one part that is independent of the directed flow (in the following denoted as diffusion) and into another part which is directly related to the flow process. The latter one is called velocity distribution. It may originate from the flow itself, e.g., from eddies, or from the finite resolution of the experiment resulting in a non-uniform velocity within one volume element (voxel). The most interesting origin for the velocity distribution are differences in mobility, i.e., different species, without spectroscopic resolution in the sample respond in different ways to the driving force that induces the motion. One reason for such differences could be a distribution of molecular weights, a common feature of polymers. The velocity distribution can be correlated to the molecular properties of the sample, however, in order to obtain the pure velocity distribution it must be clearly separated from the diffusion part.

The traditional evaluation of the experimental data is based on assumptions: high velocities and broad distributions allow to neglect the diffusion. On the other hand, at very low velocities their distribution can be

* Corresponding author. Fax: +49-351-4658-362.

E-mail address: scheler@ipfdd.de (U. Scheler).

neglected and the signal attenuation or linewidth after Fourier transform, respectively, is assigned completely to the diffusion. Obviously, this way fails in an intermediate range where both contributions are of comparable size. In other cases the velocity distribution itself is the parameter of interest, e.g., its correlation to mobility or molecular weight distribution. Then, a dominant diffusion would prevent the determination of the velocity distribution. In certain cases a deconvolution of the velocity distribution with diffusion and the distribution of pure diffusion might be possible. Deconvolution is the numerical inversion of a convolution equation, i.e., the numerical determination of f from an equation $f * g = h + \{\text{noise}\}$, given g and the right-hand side of the equation. This deconvolution is an ill-posed problem that has no unique solution. In the case of real data including noise it can only be solved using additional constraints or extra boundary conditions. In the case of data with considerable noise, if one is not careful in the choice of a numerical method, the computed approximate solution is likely not to have a continuous dependence on the given data.

An experimental alternative is proposed in the following. Because the diffusion does not depend on the driving force whereas the velocity distribution does the latter one can be obtained purely by incrementing the driving force. The attenuation of the signal between the increments is only caused by the velocity distribution, thus much weaker and very low velocities become measurable, which only cause a very slight phase modulation that is easily covered by diffusion.

This strategy has successfully been applied to electrophoresis NMR [5,6]. Here the driving force is an electric field with the strength \mathcal{E} . The velocity of the particles is related to \mathcal{E} via their electrophoretic mobility μ , where often μ is the objective of the experiment. Its distribution can be correlated (for instance) to the polydispersity and charge distribution of the particles in the sample. The displacement originating from μ (or \mathcal{E}) is of similar size as that originating from diffusion. It does not matter that the distribution of diffusion coefficients also depends on molecular weight. The contribution of all diffusion effects are kept constant. The distribution of mobility as a superposition of charge distribution and size distribution is measured. Other experiments will work in a similar way provided that the driving force is under experimental control. That is the case for mechanically driven motion like pressure driven flow in tubes or the flow caused by shearing forces as discussed for the rheometer cell below.

2. Background

In PFG NMR the position of a spin is encoded by magnetic field gradient pulses. The motion of a spin is

tracked, comparing its positions at two times. Depending on its velocity \vec{v} as well as on evolution time Δ , gradient strength g and duration δ the spin accumulate a residual phase φ according to Eq. (1) with γ the gyromagnetic ratio

$$\varphi = 2\pi\gamma\delta\Delta\vec{g} \cdot \vec{v} = 2\pi\vec{q} \cdot \vec{v} \quad (1)$$

q has been introduced as the Fourier conjugate of velocity [2]. The measured signal does not originate from a single spin but from an ensemble average. A distribution of velocities—usually described as $P(\vec{v})$ —results in a distribution of phases. The effective signal intensity E is the ensemble average of the transverse magnetization $\langle \exp(i\varphi) \rangle$ using $P(\vec{v})$ as distribution function (Eq. (2)). As a result of normalizing to $E(\vec{q} = 0)$ relaxation effects are eliminated

$$\begin{aligned} E(\vec{q}) &= \frac{E'(\vec{q})}{E(\vec{q} = 0)} = \langle \exp(i\varphi) \rangle \\ &= \int_{-\infty}^{\infty} P(\vec{v}) \exp(i2\pi\vec{q} \cdot \vec{v}) d\vec{v}. \end{aligned} \quad (2)$$

Due to the mathematical form of E of a single spin the signal intensity $E(\vec{q})$ of the spin ensemble and $P(\vec{v})$ are Fourier conjugates. In the case of pure diffusion $P(\vec{v})$ is usually of Gaussian shape. Its effect on $E(\vec{q})$ is an amplitude modulation. For ideal flow, i.e., without any diffusion nor velocity distribution, $P(\vec{v})$ is a delta function, resulting in a pure phase modulation of $E(\vec{q})$ [3].

Taking into account that the overall distribution $P(\vec{v})$ for a realistic flowing liquid is a convolution of its parts, the diffusion ($P_{\text{diff}}(\vec{v})$) and the velocity distribution plus the coherent directed motion which are both combined in $P_{\text{flow}}(\vec{v})$, Eq. (2) can be rearranged. The overall signal intensity is the product of its contributions $E_{\text{diff}}(\vec{q})$ and $E_{\text{flow}}(\vec{q})$:

$$\begin{aligned} E(\vec{q}) &= \int_{-\infty}^{\infty} (P_{\text{diff}}(\vec{v}) \otimes P_{\text{flow}}(\vec{v})) \exp(i2\pi\vec{q} \cdot \vec{v}) d\vec{v} \\ &= \left(\int_{-\infty}^{\infty} P_{\text{diff}}(\vec{v}) \exp(i2\pi\vec{q} \cdot \vec{v}) d\vec{v} \right) \\ &\quad \times \left(\int_{-\infty}^{\infty} P_{\text{flow}}(\vec{v}) \exp(i2\pi\vec{q} \cdot \vec{v}) d\vec{v} \right) \\ &= E_{\text{diff}}(\vec{q}) E_{\text{flow}}(\vec{q}). \end{aligned} \quad (3)$$

Now, both contributions to $P(\vec{v})$ can be separated making use of their main distinction: The diffusion—at constant sample temperature—to first-order is independent of the effective velocity. The absolute width of the velocity distribution increases with increasing effective velocity. The obvious solution to the problem is incrementing velocity instead of incrementing gradient strength. Doing so, the resulting phase modulation is not affected. Because \vec{q} and \vec{v} are Fourier conjugates, the phase modulation depends on their product. The

contribution of diffusion $E_{\text{diff}}(\vec{q})$ does not depend on \vec{v} , so it is the same in each slice of the experiment and can be seen as a pre-factor. This is quite similar to the fact that the T_2 relaxation time does not matter in PFG experiments performed at constant delay experiments [7]. The decrease of intensity from one slice to the next is only caused by the increasing width of the velocity distribution, fully described in $E_{\text{flow}}(\vec{q})$.

3. Experimental

All measurements have been performed at a Bruker Avance 300 NMR spectrometer at a Larmor frequency of 300 MHz for protons. The spectrometer was equipped with a microimaging accessory permitting a maximum gradient strength of 1 T/m along three axes. A 30 mm birdcage resonator mounted on a microimaging probe micro2.5 has been used, accommodating a room temperature rheometer cell driven by a stepper motor controlled by a dedicated motor control unit from Callaghan and Fischer [8] to form the flow field in water, which has been doped with CuSO_4 to permit rapid recycling. The inner diameter of the stator is 19 mm. A rotor with a diameter $d_{\text{rotor}} = 13$ mm was built to obtain a broader gap. In Fig. 1 the cross-section of the cell is depicted.

The flow imaging experiment has been performed at a rotor speed v_{rotor} of 0.1 Hz (≈ 0.4 cm/s circumferential speed). The 3D flow pulse sequence including flow compensation based on Blümich and coworkers [9] was used to encode the velocity in y direction, with frequency encoding and phase encoding for the x and y coordinates, respectively. Two hundred and fifty-six pixel in read and sixty four pixel in phase direction determine a

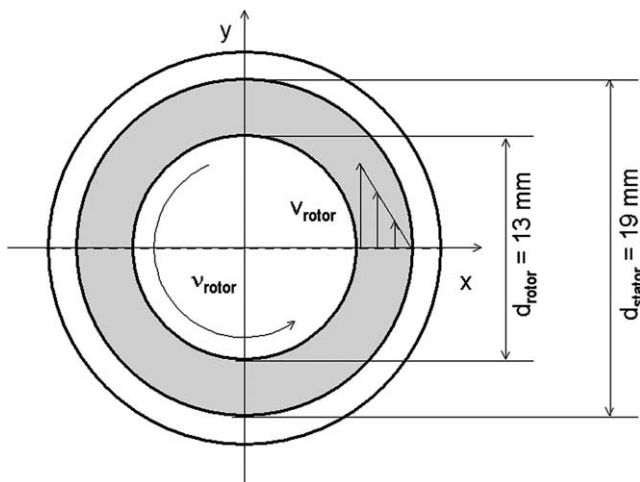


Fig. 1. Scheme of the Couette cell and the dimensions used here; dashed line: equator ($y = 0$), used for the representative velocity profiles. (The equator is a theoretical line. Voxels are of finite size and therefore they cover a certain volume around this line.)

digital resolution of $0.12 \text{ mm} \times 0.47 \text{ mm}$ (field of view 30 mm). A slice of 5 mm in z direction has been selected using a soft π pulse, Gaussian shaped. The strength of the flow encoding gradient has been incremented in 64 steps from -0.94 to 0.93 T/m. Its duration δ was 0.68 ms, the evolution time Δ 11.76 ms. The pulse sequence is shown in Fig. 2a.

In the modified experiment (Fig. 2b) the strength of the flow encoding gradient was kept constant while in the third dimension the velocity of the inner cylinder (the rotor) in the Couette cell has been incremented. The parameters (delays, pulses, and gradients) had been optimized in the flow imaging experiment and then kept for the modified version. The strength of the flow gradient was 0.46 T/m (about the half of the maximum gradient at the first experiment). The rotor speed was incremented from 0 to 0.48 Hz (2 cm/s at the rotor surface) in 30 steps. The procedure was repeated with the inverted flow gradient to simulate negative velocities necessary for the determination of the sign of the flow.

The Reynolds number is $Re = va\rho/\eta \approx 20 \times 10^{-3} \text{ m s}^{-1} \times 2.5 \times 10^{-3} \text{ m} \times 10^3 \text{ kg m}^{-3}/10^{-3} \text{ Pa s} \approx 50$, where a is the gap width, ρ and η density and viscosity of water, respectively. For a plane Couette flow critical values for Re are experimentally found in the range of some 10^2 [10]. The cylindrical Couette flow is typically described by the Taylor number $Ta = r_{\text{rotor}}(2\pi v_{\text{rotor}})^2 a^3 \rho/\eta$. Taylor vortices are expected above the critical

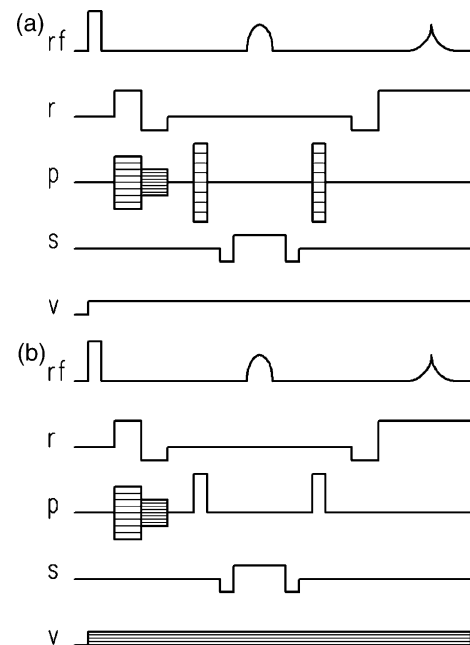


Fig. 2. Pulse sequences of the standard flow imaging experiment with incremented flow gradient (a) and the modified version with a constant flow gradient (b). r Specifies the read direction which was oriented in x here, p is the phase direction (here in y), and s the slice direction (slice gradient in z , that means the slice is parallel to the xy -plane). The bottom line v is the velocity of the rotor which is constant in a and incremented in b .

value 3×10^4 [11]. A Reynolds number of about 50 and a Taylor number of about 600 which have been calculated for the setup presented here should be low enough to ensure a laminar flow. And so it was found experimentally as shown below. Then, the velocity distributions at different rotor speeds are similar—an important prerequisite for the approach proposed. An other question is the linearity of the profile. The gap is relatively large. On the other hand, the ratio between stator and rotor diameter is below 2 and so the deviation from linearity can be neglected.

The data obtained have been processed in the same way for both experiments. The phase dimension was zero filled to 128. After the Fourier transform of both spatial dimensions the equator slice was chosen (the 65th row in phase direction, see Fig. 1). In all voxels situated here for laminar flow coherent motion takes place in y -direction only and the encoding of flow in one direction, just in y , contains all necessary information about the velocity profile. The effect of the finite voxel size is examined in the discussion. For each voxel inside the gap the real part and the magnitude of the intensity were fitted with damped cosine (Eq. (4a)) and a Gaussian distribution (Eq. (4b)), respectively. The variables q' and Δu are introduced below, ϕ is an arbitrary phase shift

$$\text{Re}(E(q')) = A \cos(2\pi q' + \phi) \exp(-q'^2 \Delta u^2 \pi^2 / (2 \log(2))), \quad (4a)$$

$$|E(q')| = A \exp(-q'^2 \Delta u^2 \pi^2 / (2 \log(2))). \quad (4b)$$

4. Results

In the flow NMR experiment \vec{q} is scanned incrementing the gradient strength. In a similar way in the

new experiment the velocity \vec{v} is incremented indirectly by controlling the velocity of the inner cylinder in the Couette cell. The velocity (the local as well as the mean velocity) is related to the driving force by means of a function that depends on the type of the experimental setup.

Here, in the rheometer cell the driving force is the rotor velocity v_{rotor} . Mean velocity and velocity distribution as a function of radius are the objectives of the experiments. To correlate v_{rotor} with these quantities a new function \vec{u} is introduced as a dimensionless velocity. It contains the spatial dependence, the distribution and all other unknown parameters (Eq. (5a)). In a next step all known and controllable parameter (\vec{g} , δ , Δ , and v_{rotor}) are combined in a further new variable \vec{q}' (Eq. (5b)). Doing so, \vec{q}' and \vec{u} become Fourier conjugates (Eq. (5c)) simplifying the data processing as well as the comparison between the classical and the modified experiment

$$\vec{v} = v_{\text{rotor}} \vec{u} \quad \text{with} \quad v_{\text{rotor}} = v_{\text{rotor}} \pi d_{\text{rotor}}, \quad (5a)$$

$$\vec{q}' = \vec{q} v_{\text{rotor}}, \quad (5b)$$

$$\exp(i2\pi \vec{q}' \cdot \vec{v}) = \exp(i2\pi \vec{q}' \cdot \vec{u}). \quad (5c)$$

Figs. 3a–c show the typical phase and amplitude modulation at selected voxels. Real and imaginary part as well as magnitude are plotted vs. \vec{q}' . The rotor speed is set as second x -axis on the top. Note: in the present case negative rotor velocities were simulated by inverting the flow encoding gradient. To assess the result it has to be compared to the classical flow experiment as shown in Figs. 4a–c for the same positions. Here again the data are plotted vs. q' and the second abscissa on the top represents that parameter that really was incremented, i.e., the gradient strength g .

In both experiments the frequency of the phase modulation increases when the distance to the rotor is reduced corresponding to the increasing velocity there.

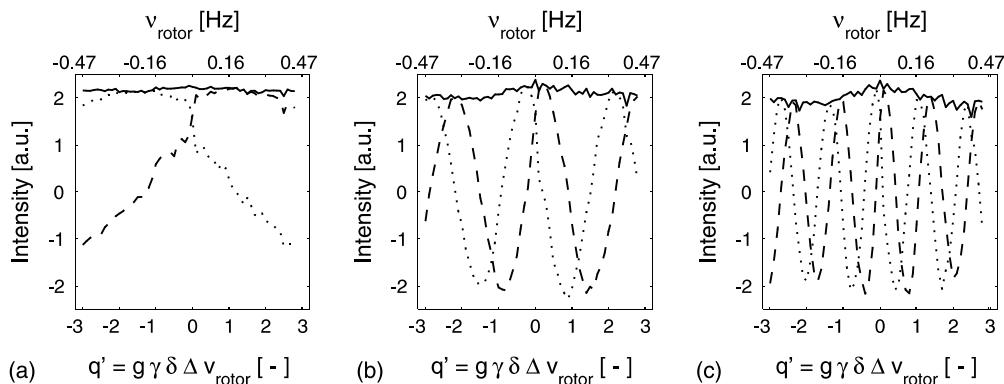


Fig. 3. Real part (—), imaginary part (·····) and magnitude (-----) for three selected voxel plotted vs. normalized q' . The rotor speed was incremented from -0.48 to $+0.48$ Hz in steps of 0.016 Hz. This is set as second x -axis on the top of the diagrams. The strength of the flow encoding gradient was 0.46 T/m, its duration 0.68 ms, evolution time 11.76 ms. (a) Voxel #57 near the stator wall, (b) voxel #65 in the middle of the gap, and (c) voxel #73 near the rotor. Increasing velocity near to the rotor results in a stronger phase modulation. Increasing q' results only in a very weak attenuation of the amplitude.

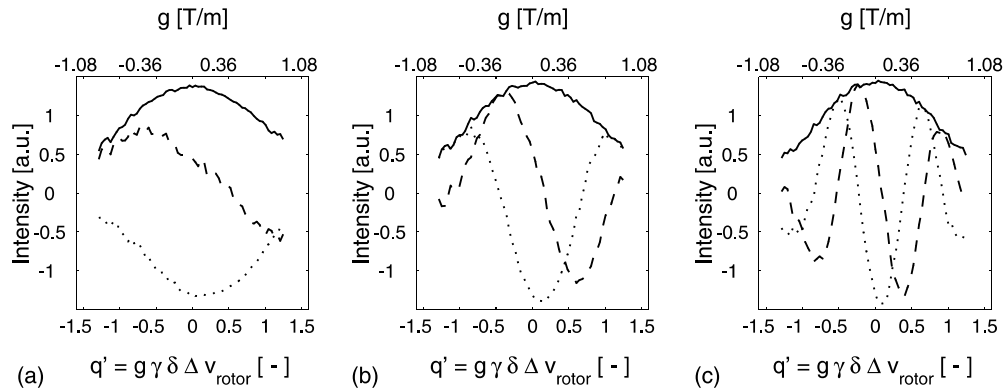


Fig. 4. Real part (—), imaginary part (·····) and magnitude (-----) for three selected voxel plotted vs. normalized q' . The strength of the flow encoding gradient was incremented from -0.94 to $+0.93$ T/m in 64 steps (second x -axis on the top of the diagrams), its duration was 0.68 ms, evolution time 11.76 ms, and the rotor speed 0.1 Hz. (a–c) Represent the same voxels as in Fig. 3. As the increasing velocity near to the rotor results in a stronger phase modulation. Increasing q' results in a substantial attenuation of the amplitude.

Moreover, at a given position the frequency in terms of the normalized q' -axis is the same for both experiments. In contrast the attenuation with increasing $|q'|$ depends on both, the type of experiment and the distance to the rotor. The first dependence is clearly visible, when incrementing the rotor speed the attenuation is much less pronounced than when incrementing the gradient strength. The dependence on the position is only slight but unambiguous. Near to the rotor the magnitude decreases somewhat faster and the statistics becomes worse.

Fig. 5 shows a direct comparison of the data from Figs. 3b and 4b. In this figure the difference in the magnitude and the agreement in the phase modulation become obvious. The intensity is normalized to voxels of the same g and v_{rotor} . The parameters are $g = 0.46$ T/m what was set for v -incrementing and reached in slice #49 for g -incrementing and $v_{\text{rotor}} = 0.1$ Hz what was given

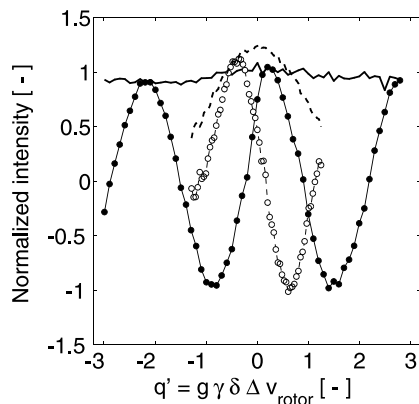


Fig. 5. Comparison of both experiments, v -incrementing (solid lines and circles connected) and g -incrementing (dashed lines, open circles connected). Real part (connected circles) and magnitude (lines) for voxel #65 plotted vs. normalized q' . Parameter see Figs. 3 and 4. The stationary surface is at the left and the rotating surface on the right.

for g -incrementing and reached in slice #38 for v -incrementing.

To get the whole profile, consisting of mean velocity and width of the velocity distribution for each voxel on the equatorial plane (Fig. 6), the data have been processed as described in Section 3. The cosine fits have

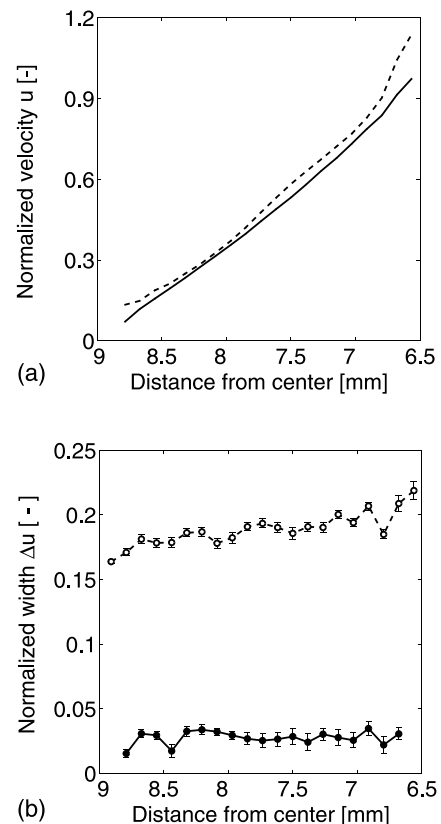


Fig. 6. Comparison of both experiments, v -incrementing (solid lines and circles) and g -incrementing (dashed lines, open circles). Profile, i.e., normalized mean velocity u (a) and normalized width Δu (b) along the equatorial radius obtained by cosine fitting (Eqs. 4a,4b).

been performed vs. q' . Thus the obtained velocity is normalized to the rotor speed v_{rotor} and hence ranges between zero and unity for both experiments. The width is also related to v_{rotor} and much smaller in the case of incrementing velocity than for the classical flow imaging experiment.

5. Discussion

The matching of the profiles in Fig. 6a and the fact that they are ranging between zero and unity, justifies the approach and the equivalence of incrementing gradient strength and incrementing the drive shaft velocity for the resulting phase modulation. Both profiles are mainly linear—in spite of the relatively wide gap. The width of the velocity distribution increases slightly for smaller distances from the rotor in the case of incremented gradients. This fact is probably due to averaging slightly different voxels: voxels close to the inner cylinder contain more contributions from species that move not exactly in y -direction than voxels at the outer cylinder wall. This is not a contradiction to the previous statement, that on the equator only y -directed flow takes place, it is a consequence of the finite spatial resolution. The equator is a theoretical line. The voxels cover a certain volume $((120 \times 470) \mu\text{m}^2 \times 5 \text{mm})$ around this line. Esp. the nearly 0.5 mm in y -direction are relevant to this discussion. The curvature of the rotor is higher than that of the stator. Therefore voxels near to the rotor cover a broader velocity range.

The flow is laminar in agreement with the low Reynolds number which can be concluded from the width of the velocity distribution as stated below. Additionally it can be concluded from the complete velocity field $(v_y(x, y))$ which has been measured: within the experimental resolution there is no y -flow on the meridian $(v_y(x = 0, y) = 0)$. From this we conclude there is no x -flow on the equator $(v_x(x, y = 0) = 0)$. The problem is the finite size of the voxels.

The fitting results of the frequency of the classical experiment is less defined because there is a lower number of oscillations in the measured q' -range. We did not expand the q' - or q -range to keep both experiments comparable. Just this low number of oscillations is the problem when measuring even lower velocities: the signal decays due to diffusion before a usable number of oscillations took place. The main advantage of the proposed approach is to enable the measurement of such low velocities or the parameter that describes the mobility, respectively. Using experiment parameters (g , Δ , δ , and so on) for which a finite intensity is detectable, the velocity can be increased stepwise without a considerable attenuation but with a significant phase modulation which frequency defines the mobility describing parameter, i.e., the response of the particles on the driving force.

The cost of this advantage is an averaging of the distribution of information. When the distributions for different rotor speeds (in each of the voxels) are similar there is no loss in information, otherwise there is. A second problem related to the distribution is even to get it. The very slow decline complicates the evaluation. For the results shown here the fitting is additionally complicated by the non-monotone dependence of the magnitude vs. increasing $|q'|$. In order to compare both experiments both results were fitted with the same equation albeit the insufficient fitting for the incremented velocities. So, the error bars are quite large and in contrast to the classic flow imaging experiment the increase of the width with decreasing distance to the rotor is not observed. Though, in Fig. 3 a trend like this might be visible: in the middle range ($|v_{\text{rotor}}| < 0.2 \text{ Hz}$) the maximum of the magnitude becomes more pronounced near the rotor.

Regardless of the discussion above about details in the velocity distribution—its width is much smaller when the driving force is incremented instead of the gradient proving the dominance of the diffusion. It is not bigger than the rise of u from one voxel to the next (Fig. 7). That means the averaging over the volume elements is the major origin for the measured distribution in the present case here confirming the flow is really laminar.

Finally the width (at least its magnitude) thus obtained shall be compared to the corrected width obtained from the traditional flow experiment. As discussed in Section 2 the overall velocity distribution is a convolution of its parts. Consequently, the part resulting from velocity can be obtained by deconvolution of the overall and the diffusion part. The first is the result of the traditional experiment at a given finite rotor speed, the second is the corresponding result at zero rotor speed. Here, instead of a complete deconvolution only the difference of both widths is calculated. To

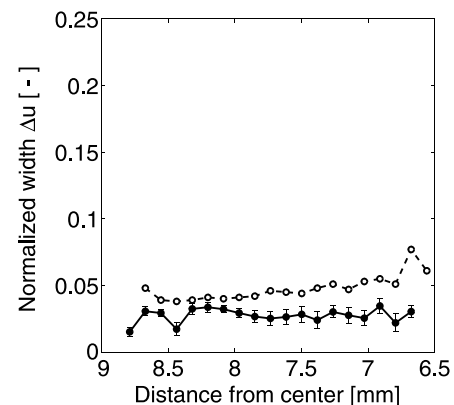


Fig. 7. Normalized width Δu of the velocity distribution along the equatorial radius obtained by v -incrementing (filled circles, see Fig. 6) compared to the difference in u between adjacent voxels (open circles) approximating the average over the voxels.

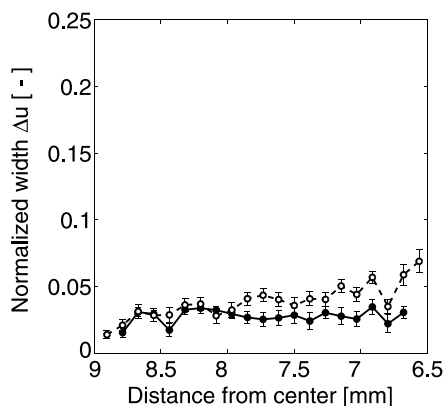


Fig. 8. Normalized width Δu of the velocity distribution along the equatorial radius obtained by v -incrementing (filled circles, see Fig. 6) compared to the normalized difference Δu_{corr} (open circles) between Δv at 0.1 Hz and Δv_{diff} at zero speed (Eq. (6)).

compare it to the modified experiment it has to be normalized as follows:

$$\Delta u_{\text{corr}} = \frac{\Delta v_{\text{corr}}}{v_{\text{rotor}}} = \frac{\Delta v_{\text{flow}} - \Delta v_{\text{diff}}}{v_{\text{rotor}}} = \Delta u_{\text{flow}} - \frac{\Delta v_{\text{diff}}}{v_{\text{rotor}}}, \quad (6)$$

where Δu_{corr} is the corrected and normalized width, Δv_{corr} the corrected width in cm/s, Δv_{flow} the width in cm/s obtained in the classic experiment at v_{rotor} and Δu_{flow} the corresponding normalized width. Δv_{diff} , the width in cm/s at zero rotor speed, is independent of the position 0.06 cm/s. So, the correction term is for $v_{\text{rotor}} = 0.1$ Hz: $0.06 \text{ cm s}^{-1} / (0.1 \text{ Hz} * 1.3 \text{ cm} * \pi) = 0.15$. In Fig. 8 Δu_{corr} for this speed is compared to Δu , obtained by incrementing velocity. In the error margin the widths are of comparable magnitudes confirming again the correctness of the proposed approach.

6. Conclusions

An experimental approach has been demonstrated, which allows the measurement of very slow velocities and of the distribution of the mobility, the response to the driving force. While in the conventional flow experiment the gradient strength is incremented, here the driving force is incremented during the experiment. All displacements of the spins—by directed flow as well as by diffusion—influence the signal. With increasing gradient the signal is modulated in phase due to flow and it decreases due to diffusion. For very slow flow the phase modulation is very weak and easily covered by the attenuation due to diffusion. For these cases an alternative experiment is suggested. There the effect of diffusion is constant because the gradient strength is kept constant.

A phase modulation is obtained by incrementing the velocity or the driving force, respectively. The response to the driving force, the mobility, is obtained from this modulation. The distribution of mobilities in the sample attenuates the signal. And this attenuation is only due to this distribution not due to diffusion and mobility distribution as in the conventional flow experiment.

It has been demonstrated that this approach works for the rotor driven flow in a rheometer cell. For the very slow flow discussed here the diffusion is dominant, although not as high that it would completely cover the phase modulation. The distribution of the directed flow is mainly caused by averaging over the volume elements. The obtained normalized width correspond quite well to its conventional estimation by subtracting the width at zero rotor speed.

Future steps are on the one hand measuring higher velocities up to turbulent flow and, hence, to broader velocity distributions. On the other hand instead of the master velocity the driving torque in rheometer has to be controlled (and measured). This approach will yield indeed rheological relevant data like viscosity and its shear-dependence directly.

Acknowledgments

The authors thank the BMBF for financial support under Grants 03N8624 and 03N8623 as well as Prof. Paul T. Callaghan for the rheometer cell as well as for help on starting this device.

References

- [1] P.T. Callaghan, Principles of Nuclear Magnetic Resonance Microscopy, Clarendon Press, Oxford, 1991.
- [2] B. Blümich, NMR Imaging of Materials, Clarendon Press, Oxford, 2000.
- [3] E.O. Stejskal, J.E. Tanner, J. Chem. Phys. 42 (1965) 288.
- [4] J. Kärgler, G. Fleischer, U. Roland, in: J. Kärgler, P. Heitjans, R. Haberlandt (Eds.), Diffusion in Condensed Matter, Vieweg, Braunschweig, 1998.
- [5] U. Scheler, in: S.K. Tripathy, J. Kumar, H.S. Nalwa (Eds.), Handbook of Polyelectrolytes and their Applications, American Scientific Publishers, 2002.
- [6] M. Holz, in: J. Kärgler, P. Heitjans, R. Haberlandt (Eds.), Diffusion in Condensed Matter, Vieweg, Braunschweig, 1998.
- [7] S. Emid, J.H.N. Creyton, Physica 128B (1985) 81.
- [8] P.T. Callaghan, E. Fischer, Bruker-Report 149 (2001) 34.
- [9] S. Laukemper-Ostendorf, K. Rombach, P. Blümmler, B. Blümich, NMR Imaging of Stationary Flow, BRUKER Application Note, 1996.
- [10] L.S. Tuckerman, D. Barkley, Theor. Comput. Fluid Dyn. 16 (2002) 91.
- [11] F. White, Viscous Fluid Flow, Mc Graw-Hill, New York, 1974.